Sulfidation and Reoxidation of U(VI)-Incorporated Goethite: Implications for U Retention during Sub-Surface Redox Cycling

Stagg, O.; Morris, K.; Townsend, L. T.; Kvashnina, K.; Baker, M. L.; Dempsey, R.; Abrahamsen-Mills, L.; Shaw, S.;

Originally published:

November 2022

Environmental Science and Technology 56(2022)24, 17643-17652

DOI: https://doi.org/10.1021/acs.est.2c05314

Sulfidation of U(VI)-incorporated goethite

Olwen Stagg,[1] Katherine Morris,[1] Luke T. Townsend,[1,†] Kristina Kvashnina,[2] Michael L. Baker,[3] Ryan Dempsey,[3] Liam Abrahamsen-Mills[4] and Samuel Shaw[1]*

[1]Research Centre for Radwaste Disposal and Williamson Research Centre for Molecular Environmental Science, Department of Earth and Environmental Sciences, The University of Manchester, Manchester, M13 9PL, U.K.

[2]The Rossendorf Beamline at ESRF – The European Synchrotron, CS40220, 38043 Grenoble Cedex 9, France.

[3]Department of Chemistry, The University of Manchester, Manchester, M13 9PL.

[4]National Nuclear Laboratory, Warrington, Cheshire, WA3 6AE, U.K.

KEYWORDS

Sulfidation; Uranium; Iron (oxyhydr)oxides; XAS; Persulfide

SYNOPSIS

Reaction of U(VI)-goethite with aqueous sulfide results in transient remobilization of trace levels of aqueous uranium, with long-term solid phase retention of U(IV)O_2.

ABSTRACT

Over 60 years of nuclear activities have resulted in a global legacy of contaminated land and radioactive waste. Uranium (U) is a significant component of this legacy and is present in radioactive wastes and at many contaminated sites. U-incorporated iron (oxyhydr)oxides may provide a long-term barrier to U migration in the environment. However, reductive dissolution of iron (oxyhydr)oxides can occur on reaction with aqueous sulfide (sulfidation), a common species in contaminated land and radioactive waste disposal scenarios due to the microbial reduction of sulfate. In this work, U(VI)-goethite was initially reacted with aqueous sulfide, followed by a reoxidation reaction, to further understand the long-term fate of U species under fluctuating environmental conditions. Over the first day of sulfidation, a transient release of aqueous U was observed, likely due to intermediate uranyl(VI)-persulfide species. However, overall U was retained in the solid phase, with the formation of nanocrystalline U(IV)O_2 in the sulfidised system, along with a persistent U(V) component. On reoxidation, U was predominantly associated with an iron (oxyhydr)oxide phase, either as an adsorbed uranyl (approximately 65%) or an incorporated U (35%) species. These findings support the overarching concept of iron (oxyhydr)oxides acting as a barrier to U migration in the environment.

Abstract Art

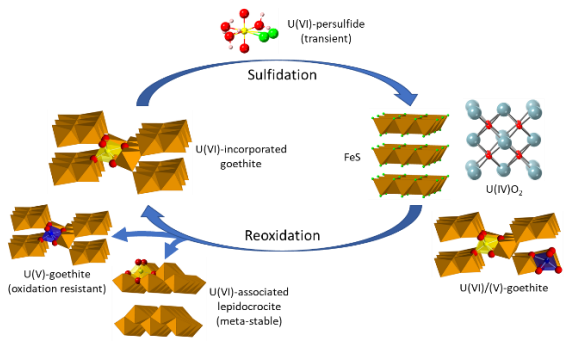

INTRODUCTION

Globally, U is considered a key environmental contaminant, prevalent in the sub-surface at numerous nuclear legacy sites (e.g. Hanford, Rifle, Oak Ridge).[1–4] U is also prevalent in higher activity radioactive wastes that are destined for disposal in a deep underground geological disposal facility (GDF).[5] To aid long term containment, a GDF will contain a multi-barrier design to limit radionuclide migration from the facility over geological timescales.[1,2,5] In addition to naturally present minerals from the surrounding host rock of the GDF, the corrosion of engineering iron and steel structures will lead to iron (oxyhydr)oxide phases (e.g. magnetite, goethite, green rust) being ubiquitous in and around the facility.[6–8] Previous studies have shown that iron (oxyhydr)oxides can readily incorporate U species into the crystal structure and may therefore act as an additional barrier to U migration in the environment over timescales relevant to a GDF.[9–23] However, the subsurface biogeochemistry of both contaminated land environments and GDF scenarios will evolve over time, and this may include redox cycling induced by the onset of sulfate reducing conditions or by oxygen ingress.[2,24] Consequently, U-associated iron (oxyhydr)oxide phases may react with aqueous sulfide, known as a sulfidation reaction.[25,26] Potential reoxidation may then occur over the longer term, with cycling between reduced and oxidised sates likely.[27,28] Therefore, given the potential for these fluctuating biogeochemical cycles in the subsurface, the end-fate of incorporated radionuclides (including U) is unclear.

Under environmental sub-surface conditions, the migration of U species is often dominated by changes in redox potential, with oxidation state a major control on U mobility.[4] Under circumneutral conditions in the subsurface, U generally exists as either U(VI) or U(IV) under oxic and anoxic conditions, respectively.[2,4,29] U(VI) typically forms the relatively mobile uranyl ion ($UO_2^{2+}{}_{(aq)}$), whereas U(IV) may form poorly soluble phases of either non-crystalline U(IV) or

nanoparticulate uraninite (UO_2).[2,4,29] In addition, although U(V) can undergo disproportionation to U(IV) and U(VI),[30] recent studies have indicated that U(V) can be formed and stabilised during a number of biogeochemical processes in the environment.[31,32] In particular, U(V) can be stabilised on incorporation into iron (oxyhydr)oxide phases,[9,13,15–17,19,20] and U(VI)-incorporated iron (oxyhydr)oxides may undergo reduction to U(V)-incorporated phases.[19,21]

The formation of U-incorporated iron (oxyhydr)oxide phases is thought to occur *via* substitution of U(VI/V) for an Fe(III) site within the mineral structure, potentially immobilising U in the long-term.[9,13,15–21,33] Iron (oxyhydr)oxide mineral phases are ubiquitous in engineered and natural environments, commonly forming *via* the breakdown of Fe-containing silicate minerals, by the oxidation of dissolved ferrous iron, and during metal corrosion in engineered systems (e.g. contaminated land and GDF scenarios).[34,35] Iron (oxyhydr)oxides in engineered and natural environments may be subject to fluctuating redox conditions, such as oxygen ingress or the onset of iron reducing conditions.[4,36–38] Additionally, in many subsurface scenarios (e.g. organic-rich sediments), microbial sulfate reduction may occur, in turn producing aqueous sulfide species.[2,24,39,40] The resulting sulfide may then react with iron (oxyhydr)oxide phases in a process known as sulfidation, where reductive dissolution occurs at the mineral surface, releasing Fe(II) into solution.[25,41] Consequently, the released Fe(II) may then react with HS^- to form secondary iron sulfide phases, such as mackinawite (FeS), which in turn may influence the behaviour and fate of radionuclides, including U.[42–45]

A field study in Rifle (USA) observed a release of aqueous U following the onset of microbial sulfate reduction.[24] Transient aqueous U release was also observed during abiotic sulfidation reactions, including the reaction of an abiotic sulfide solution with U(V)-incorporated magnetite,[46] U(VI)-adsorbed hematite and U(VI)-adsorbed lepidocrocite.[47,48] These abiotic studies suggested

that U release may be a result of poor U(VI) affinity for a sulfidised surface.[46–48] Further insight was provided by the sulfidation of U(VI)-adsorbed ferrihydrite, where aqueous U(VI) speciation was attributed to the formation of an intermediate uranyl(VI)-persulfide species, which had only a weak adsorption affinity for FeS.[49] However, in all abiotic systems reduction to U(IV) was observed overall, with U retained mainly as either nanoparticulate uraninite ($U(IV)O_2$)[46,48,49] or monomeric U(IV) following sulfidation.[47]

On exposure of $U(IV)O_2$ to oxygen, rapid formation and remobilization of U(VI) species typically occurs.[27,38] However, nanocrystalline mackinawite has previously been shown to protect $U(IV)O_2$ from reoxidation.[50] In this work, synthetic nanocrystalline mackinawite acted as an oxygen scavenger, transforming to nanogoethite and lepidocrocite, with no $U(IV)O_2$ dissolution observed prior to complete FeS depletion.[50] $U(IV)O_2$ oxidative dissolution (5% CO_2/2% O_2 gas mixture, 4 mM $NaHCO_3$) then led to the remobilization of aqueous U(VI)-carbonato complexes, and subsequent adsorption (25%) onto goethite/lepidocrocite. Consequently, following sulfidation, the long-term fate of $U(IV)O_2$ will be dependent on the oxygen scavenging capability of the formed amorphous FeS phase and the ambient physicochemical conditions, with carbonate concentration a significant control.[50] Simultaneous reoxidation of FeS and $U(IV)O_2$ may therefore result in partial U(V,VI) incorporation into the forming iron (oxyhydr)oxide phase. Alternatively, oxygen scavenging may occur, as already observed with nanocrystalline mackinawite,[50] thereby delaying $U(IV)O_2$ reoxidation and potentially preventing U(V,VI) incorporation into newly formed Fe(III) bearing (oxyhydr)oxides. This may lead to delayed U oxidation, presumptively to U(VI), which would then likely be retained as a more labile adsorbed phase, with potentially higher mobility in the environment.

Given the observed transient release of U during the sulfidation of U-associated magnetite,[46] ferrihydrite,[49] hematite and lepidocrocite,[47,48] for iron (oxyhydr)oxides to be considered as long-term sequesters in subsurface environmental systems, further understanding of U behaviour during sulfidation and associated redox cycling (e.g. reoxidation) is needed. In particular, the mechanism for the transient U release during iron (oxyhydr)oxide sulfidation is still unclear, as is the long-term fate of the reduced $U(IV)O_2$ phase formed during sulfidation. Here, highly controlled sulfidation and reoxidation experiments were performed on U(VI)-incorporated goethite, using a chemostat system.[46,49] The reactions were monitored at selected timepoints using geochemical analyses (e.g. ICP-MS and colorimetric assay), X-ray absorption spectroscopy (XAS) and transmission electron microscopy (TEM). During sulfidation, a transient release (< 32 hours) of aqueous U was observed, followed by subsequent, longer term formation of $U(IV)O_2$ over several months. Interestingly, a U(V) species was also formed within a few hours of sulfidation, and persisted even after 7 months of sulfidation. Upon reoxidation, goethite and lepidocrocite formed, with U either adsorbed or incorporated into the iron (oxyhydr)oxide phase.

MATERIALS AND METHODS

Mineral preparation. U(VI)-incorporated goethite (approximately 0.2 wt% U) was formed *via* a hydrothermal synthesis method, as previously described.[21] The resultant slurry was then washed several times with DIW, and washed with 4 mM HCl to remove adsorbed U(VI).[51,52] After several more washes with DIW, the solid was left to dry overnight (40 °C), and the mineral phase confirmed by powder X-ray diffraction (XRD).

Sulfidation experiment. Experiments were performed under anoxic conditions in an Applikon Bioreactor (nitrogen atmosphere), which monitored and/or controlled the pH, Eh, temperature and

reagent additions, as required.[49] Samples were periodically collected under anoxic conditions, with all sample manipulations conducted within an anaerobic Coy cabinet under a mixed nitrogen/hydrogen (95 % : 5 %) atmosphere. A U(VI)-goethite slurry was prepared (400 mL, 1 g/L) and transferred to the Applikon Bioreactor under a flow of N_2, then left to equilibrate overnight. A sodium sulfide solution (0.4 M) was prepared in the Coy cabinet from sodium sulfide nonahydrate ($Na_2S.9H_2O$), with the concentration confirmed through methylene blue assay using the Radiello RAD171 standard.[53] The resulting sodium sulfide solution was then added to the vessel at a constant rate (0.1 mL/min) over 4 hours, to reach a final HS^-/Fe(III) molar ratio of 2:1. The experiment was kept anoxic under a constant flow of N_2, and the pH was maintained at pH 7 *via* the automated addition of 1 M HCl. The reaction was controlled in the chemostat vessel for 72 hours, and then transferred to a Schott bottle in the Coy cabinet for long-term anaerobic storage. During sulfidation, the experiment was sampled periodically and the slurry filtered to < 1.5 nm using 3 kDa Nanosep centrifugation ultrafilters (PES). The filtrate was then preserved for analysis by either acidification for cation analysis (U and Fe), or by reaction with a zinc acetate solution (82 mM) for sulfide analysis. Aqueous Fe and U were monitored by inductively coupled plasma mass spectrometry (ICP-MS, Agilent 8800), with aqueous sulfide analysed using the methylene blue assay and the Radiello RAD171 standard.[53]

For solid phase analysis, samples were studied by transmission electron microscopy (TEM), X-ray absorption spectroscopy (XAS), and X-ray emission spectroscopy (XES). For TEM, sample slurry was dropped onto TEM grids (holey C film on Au 300 mesh) and dried inside the anaerobic cabinet prior to analysis on either FEI Tecnai TF20 or FEI Titan3 Themis 300 (LEMAS). For X-ray absorption spectroscopy (XAS) analysis, solid samples were obtained by filtration (nylon membrane filter, 0.22 μm), then stored and transported at -80 °C under anoxic conditions to the

Diamond Light Source (UK) for analysis on either the I20-scanning or B18 beamline. XAS spectra were collected from the U L_{III}-edge in fluorescence mode at 80 K, using 64-element (I20) and 36-element (B18) Ge detectors. The resulting data was processed using the Demeter software package, using Athena and Artemis with FEFF6.[54] For X-ray emission spectroscopy (XES), select solid filtrate samples were transported frozen and under anoxic conditions to the European Synchrotron Radiation Facility (ESRF) in Grenoble. Measurements were performed at beamline BM20,[55] and the incident energy was selected using the <111> reflection from a double Si crystal monochromator. X-ray absorption near edge structure (XANES) spectra were measured in high-energy resolution fluorescence detected (HERFD) mode using an X-ray emission spectrometer,[56] and the sample, analyzer crystal and photon detector (silicon drift detector, Katek) were arranged in a vertical Rowland geometry. U M_{IV}-edge HERFD-XANES spectra were collected using the U Mβ emission line (~3337 eV),[57,58] under cryo conditions with Oxford Cryostream (800 series) at 50K. Subsequent data analysis was performed using the ITFA software package.[59]

Reoxidation experiment. As with the sulfidation study, the reoxidation experiment was also performed in the Applikon Bioreactor, which again monitored and/or controlled the dissolved oxygen (DO), pH, Eh, temperature and reagent additions. Subsequent sample manipulations were conducted within an anaerobic coy cabinet, under a mixed nitrogen/hydrogen atmosphere. Briefly, after 5 months of aging under anoxic conditions, the sulfidised U(VI)-goethite slurry was diluted in de-oxygenated water (0.5 g/L, 200 mL), transferred to the Applikon Bioreactor, and left to equilibrate overnight under a flow of nitrogen. The pH was maintained at pH 7 *via* additions of 50 mM HCl or 50 mM NaOH, and the reaction was initiated by the introduction of laboratory air, set to maintain a dissolved oxygen level of 5% within the solution. Samples were collected

periodically over 4 days, with aqueous (U and Fe) and solid phase (XRD, TEM, XAS) samples collected, as above, for analysis.

RESULTS AND DISCUSSION

The U(VI)-incorporated goethite was initially characterised by XRD (Figure S7), to confirm that goethite was the only crystalline phase present. Previous analysis has confirmed that U(VI) is incorporated within the goethite structure by substitution into an Fe(III) site (~0.2 wt% U), forming a distorted octahedral coordination.[21]

Sulfidation of U(VI)-goethite. Sulfidation of the U(VI)-goethite slurry (1 g/L, 11.3 mM Fe) was initiated by a controlled 4 hour addition of aqueous sulfide (22.5 mM), to reach a final HS^-/Fe(III) molar ratio of 2:1. Over the 4 hours of addition, the concentration of aqueous sulfide increased steadily to a peak of 12.1 mM at 4 hours (Figure 1), followed by a gradual decrease in aqueous concentration, with no detectable aqueous sulfide by 24 hours. During this time, aqueous Fe (presumably as Fe(II)) followed the same increase in solution concentration at low but detectable levels, with a peak of 90.1 μM at 4 hours (Figure S1). However, after aqueous sulfide had been removed (24 hours), aqueous Fe steadily increased (150 μM by 72 hours). These trends are characteristic of the reported sulfidation mechanism, with the steady decrease in aqueous sulfide from 4 hours likely due to sulfide oxidation on reaction with, and concomitant reductive dissolution of, the U(VI)-goethite.[25,41,60] However, given the excess aqueous sulfide in this system (HS^-/Fe(III) molar ratio of 2:1), it is likely that immediate precipitation of FeS occurred following the release of Fe(II) into solution, resulting in the low levels of aqueous Fe initially detected, followed by an increase in aqueous Fe after all aqueous sulfide was removed from the system. As with previous studies of U associated with iron (oxyhydr)oxides,[46,47,49] the reductive

dissolution of U(VI)-goethite also displayed a transient release of U during sulfidation (Figure 1). Specifically, the aqueous U release followed the same trend as aqueous sulfide, albeit with a slight time delay of 1-2 hours. Aqueous U increased steadily after 1 hour, with a peak of 2.5% U_{total} (0.21 µM) at 6 hours, followed by a gradual depletion over a further 26 hours. As aqueous samples were collected using 3 kDa ultrafilters (approximately equivalent to 1.5 nm pore size), released U is assumed to be an aqueous U(VI) speciation (as opposed to colloidal U).[61,62] Interestingly, past work ascribed the transient U release during U(VI)-ferrihydrite sulfidation to the formation of a uranyl(VI)-persulfide species.[49] However, it is also worth noting that the reactant slurry appeared very colloidal between 3-6 hours, despite filtering to 1.5 nm. A recent study has indicated that FeS formation may proceed *via* nanoparticulate FeS precursors, which are approximately 2 nm in size.[63] Therefore, the potential of U association with these aqueous FeS clusters cannot be completely ruled out, and there is a possibility that this transient U release was due to association with the colloidal phase.

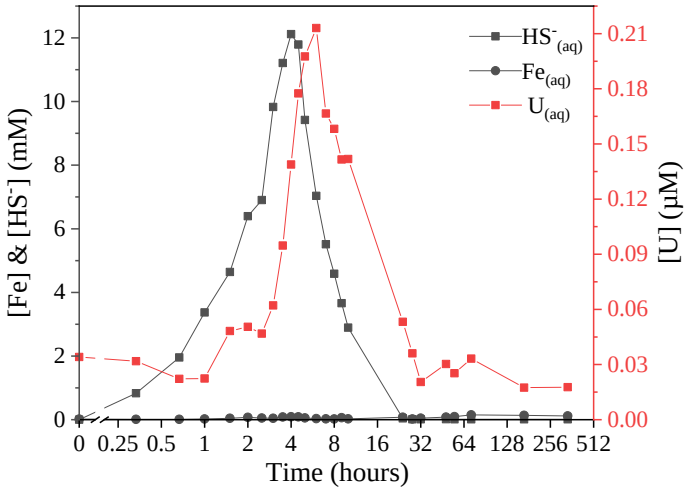

Figure 1. Aqueous Fe, HS^- and U during the sulfidation of U(VI)-incorporated goethite. The *x*-axis is shown as $\log_2$ after 0 hours.

The mineral transformations that occurred during the sulfidation of U(VI)-goethite were monitored by TEM, with images collected at selected timepoints. After 1 day of sulfidation, sheet-like particles were observed that matched well with amorphous mackinawite (FeS) morphology (Figure S8).[64] This confirms that rapid reductive dissolution of U(VI)-goethite followed by secondary FeS formation had occurred by 1 day. Furthermore, a SAED pattern collected after 7 months of aging (Figure S9) was also consistent with poorly ordered FeS.[64] However, the presence of persistent rod-shaped iron (oxyhydr)oxide phases can also be seen in the samples at 7 months (Figure S10) which are likely refractory U-goethite crystals. Overall, TEM images confirm that although rapid sulfidation and reductive dissolution of U(VI)-incorporated goethite occurred, a residual U-goethite component was still present after 7 months.

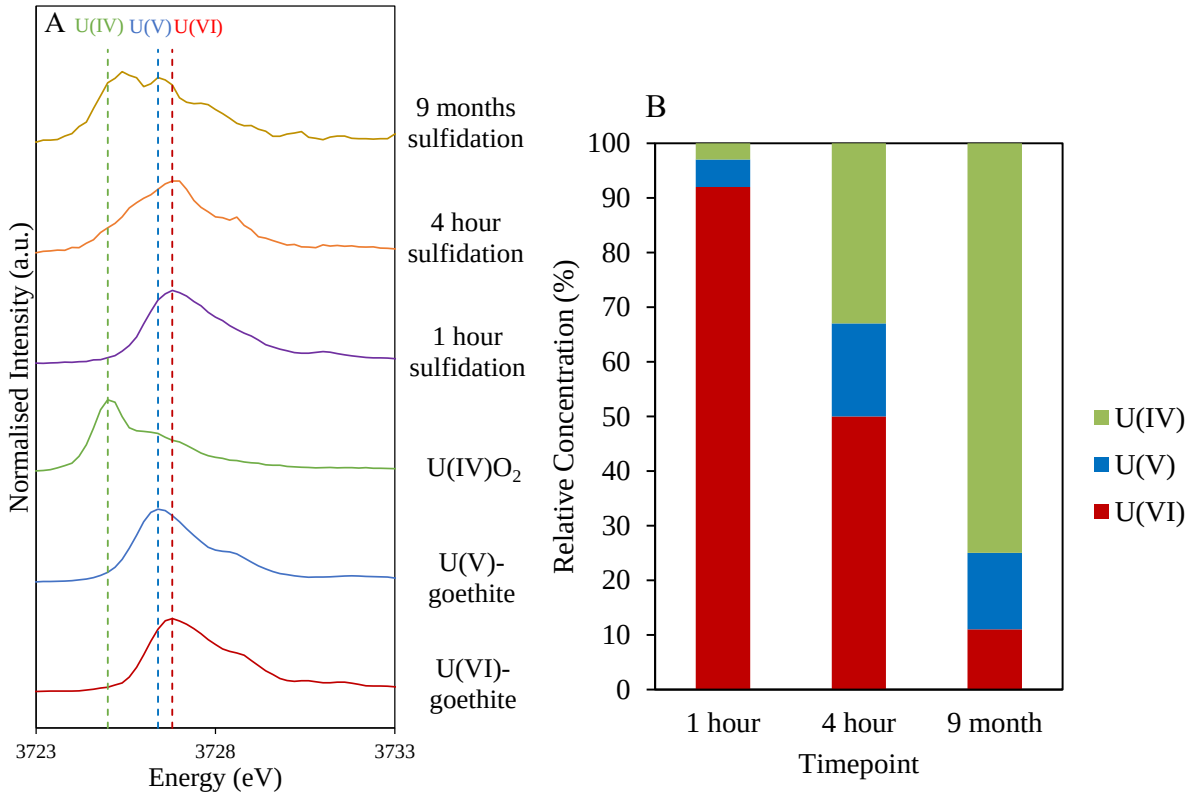

Figure 2. (A) U M_{IV}-edge HERFD-XANES, showing timepoints for U(VI)-goethite sulfidation samples. Dashed lines indicate peaks for standards $U(IV)O_2$, U(V)-goethite and U(VI)-goethite.

(B) Results from ITFA[59] of U M_{IV}-edge HERFD-XANES data, showing the relative concentrations of U(IV), U(V) and U(VI) in U(VI)-goethite sulfidation samples (further details in SI, Table S1).

To monitor U speciation during U(VI)-goethite sulfidation, XES and XAS data were collected at select timepoints. Firstly, the change in U oxidation state was measured by U M_{IV}-edge HERFD-XANES and further quantified using ITFA (full details in Table S1, SI).[59] As expected, there was a continuous decrease in U(VI) and increase of U(IV) over time, from 92% U(VI) and 3% U(IV) after 1 hour, to 11% U(VI) and 75% U(IV) by 9 months (Figure 2). Interestingly, a U(V) component was also identified, which increased from 5% at 1 hour to 17% by 4 hours, with 14% retained after 9 months. This seems to correlate with results from a recent study investigating the reduction of U(VI) by magnetite.[65] On reaction with magnetite, U(VI) was initially reduced to a mixed U(IV)/U(V) oxide phase, with the formation of U(IV)O_2 nanoparticles dominant by 4 weeks.[65] In addition, the reaction of U(VI) with FeS has previously been suggested to result in mixed valence U oxide phases, such as U_3O_8 or U_4O_9, as well as U(IV)O_2.[42,45,66] Therefore, we suggest that during the early stages of U(VI)-goethite sulfidation, FeS initially reduces U(VI), released from goethite during reductive dissolution, to a mixed valence U(IV,V) bearing oxide species (e.g. U_4O_9), with U(IV)O_2 dominant in the long-term.

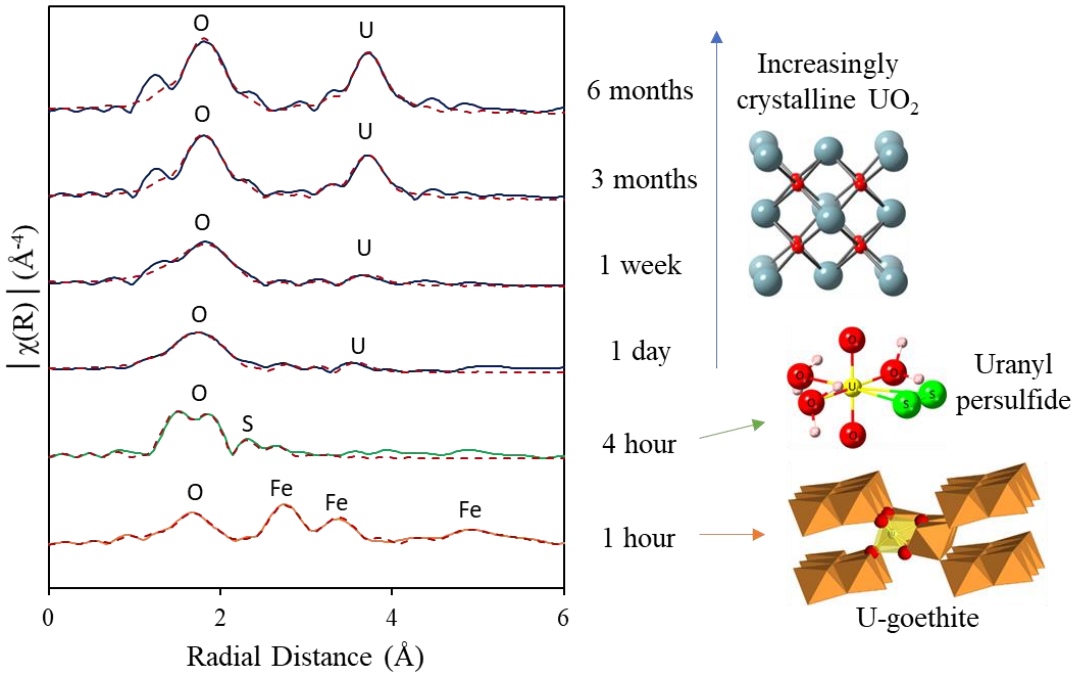

Figure 3. U L_{III}-edge XAS spectra for U(VI)-goethite sulfidation, displaying the Fourier transform of k^3-weighted EXAFS. Solid lines are data and dashed lines the modelled best fits.

The U speciation was further probed by U L_{III}-edge EXAFS fitting, to determine changes in the local coordination environment. After 1 hour of sulfidation, 4 U-O and 7 U-Fe shells were identified and validated using F-tests (Table S2, SI), with the fit matching closely to previous EXAFS studies on U(VI) incorporated into goethite.[21] Given that there is no aqueous U detected at 1 hour (Figure 1), this suggests that U is still largely incorporated within the goethite structure. However, there was a clear elongation in U-O_1 (1.82(1) Å to 1.88(1) Å)[21] possibly reflecting the formation of U(V) (which has a reported U=O bond length of 1.9 Å),[67] as indicated by ITFA analysis of the U M_{IV}-edge HERFD-XANES data (5% U(V), Figure 2). As U appears to be incorporated in goethite at this timepoint, from the U-Fe shells still present in the EXAFS fit, this suggests that an electron transfer mechanism (from either adsorbed Fe(II) or HS^-) may have partially reduced incorporated U(VI) to U(V) in goethite, as previously observed during the

reaction of Fe(II) with U(VI)-goethite.[21] By 4 hours, the best fit model had 3 U-O distances (1.85 Å, 2.11 Å and 2.29 Å) and a S backscatterer (2.67 Å), with U-Fe shells (0.5 Fe backscatterers) at 3.21 Å and 3.44 Å. The diminished occupancy of the U-Fe shells indicates a decrease in long range order in the sample, likely from the rapid reductive dissolution of U(VI)-goethite by 4 hours. The presence of the small, but essential, number of S backscatterers (0.5 S at 2.67 Å; F-test = 100%, SI Table S2) in the fit indicates the presence of a uranyl persulfide species.[49] In a previous study, DFT calculations suggested a weak adsorption affinity for uranyl(VI)-persulfide and the mackinawite surface.[49] Therefore, the formation of an aqueous uranyl persulfide complex may explain the transient release of U during the first several hours of reaction. Interestingly, this transient uranyl persulfide species has only been observed during the sulfidation of U(VI) systems (here as U(VI)-goethite, and during U(VI)-ferrihydrite sulfidation[49]), but was not observed during U(V)-magnetite sulfidation.[46] In addition, the remobilization of U to solution was relatively short-lived in the circumneutral U(VI) systems (< 32 hours, Figure 1),[49] yet for the U(V)-magnetite system U remained in solution for over a week (complete removal by 9 days).[46] A possible explanation for these observations could be related to the overall charge of the uranyl persulfide species. For U(VI), a uranyl ion (UO_2^{2+}) is bound to a disulfide species (S_2^{2-}) and coordinated by water molecules, resulting in a neutral complex that is relatively weakly bound to the FeS surface.[49] This results in a short-lived transient aqueous U species which is partially adsorbed onto the FeS surface, thereby enabling the uranyl(VI) persulfide species to be observed by EXAFS of the solid phase. However, a U(V) uranyl ion (UO_2^{+}) binding to a disulfide (S_2^{-}) species would result in a negatively charged complex, as previously modelled using DFT calculations.[49] As the point of zero charge (pzc) for magnetite is 6.55,[68] with nanomagnetite the only identified phase (by TEM) after 8 hours of reaction,[46] a negatively charged U(V)-persulfide species would be repelled from

the surface, would not be associated with the solid EXAFS sample, and may persist in the solution phase for an extended period of time, as observed during U(V)-magnetite sulfidation.[46] Overall, this suggests that although U(VI) and U(V) may both form an aqueous uranyl persulfide complex, the U(VI) species is preferentially adsorbed to the solid phase at circumneutral pH, and there is consequently only a transient release of U(VI).

Table 1. Details of the EXAFS fits for U(VI)-goethite standard, and 1-4 hours sulfidation samples (full details in SI, Table S2).*Standard taken from previous study.[21]

U(VI)-goethite*			**1 hour**			**4 hours**		
Path	R (Å)	CN	Path	R (Å)	CN	Path	R (Å)	CN
O_1	1.82(1)	0.8	O_1	1.88(1)	1	O_1	1.85(1)	1
O_2	2.03(2)	0.8	O_2	2.06(3)	1	O_2	2.11(2)	1.8
O_3	2.23 (1)	2.2	O_3	2.23(2)	2.5	O_3	2.29(2)	3.2
O_4	2.42(1)	2.2	O_4	2.40(2)	1.5	S_1	2.67(3)	0.5
Fe_1	3.22(1)	2	Fe_1	3.21(1)	2	Fe_1	3.21(5)	0.5
Fe_2	3.44(2)	2	Fe_2	3.44(1)	2	Fe_2	3.44(6)	0.5
Fe_3	3.65(1)	3	Fe_3	3.64(1)	3			
Fe_4	4.71(3)	1	Fe_4	4.70(3)	1			
Fe_5	5.32(2)	2	Fe_5	5.30(2)	3			
Fe_6	5.63(3)	2	Fe_6	5.61(2)	4			
Fe_7	5.90(4)	2	Fe_7	5.88(3)	3			

After 1 day of sulfidation, the best fit model contains 3 O backscatterers at 2.24 Å, 3 O backscatterers at 2.38 Å, 0.5 Fe backscatterers at 3.29 Å and 3.47 Å, and 1 U backscatterer at 3.71

Å, suggesting a complex mixture of uranium coordination environments and oxidation states (Table 2). Firstly, the 3 O backscatterers at 2.38 Å and the 1 U backscatterer at 3.71 Å suggest some UO_2 formation, with the low U-U coordination number indicating a poorly crystalline UO_2 phase (c.f. crystalline UO_2 with 8 O at 2.37 Å and 12 U at 3.87 Å).[62] However, the 3 O backscatterers at 2.24 Å may suggest the presence of a U_4O_9 ($U(V)_2U(IV)_2O_9$) phase (c.f. U_4O_9, U-O at 2.25 Å and U-U at 3.87 Å).[69] Therefore, this further supports the hypothesis that a mixed-valence U oxide species is present, in addition to poorly crystalline UO_2, providing a possible explanation for the U(IV) and U(V) components observed in the M_{IV}-edge HERFD-XANES spectra (Figure 2). In addition, the presence of 2 U-Fe shells at 3.29 Å and 3.47 Å indicate that a residual U-goethite phase (either U(V) or U(VI)) is retained in the system after 1 day of sulfidation. Interestingly, a persistent U(VI) component is still identified by M_{IV}-edge HERFD-XANES after 9 months (11%, Figure 2), and goethite particles are identified by TEM imaging after 7 months, which does suggest that a fraction of U(VI)-goethite is retained long-term in the system. However, as stated previously, U(VI)-goethite reportedly undergoes partial reduction to a mixed U(V)/U(VI)-goethite species on reaction with aqueous Fe(II).[21] Therefore, given that the coordination environment for both U(V)- and U(VI)-goethite include O backscatterers at approximately 2.2 Å and 2.4 Å (cf. 2.24 Å and 2.38 Å after 1 day of sulfidation), and given the highly reducing conditions in the system, both U(V)- and U(VI)-goethite incorporated species may contribute to the persistent U(V) and U(VI) components of the M_{IV}-edge HERFD-XANES spectra (Figure 2). Consequently, the presence of U(V) in the system may be due to either a partially reduced U(VI/V)-goethite species (electron transfer from aqueous Fe(II) and/or aqueous HS^-) and/or the formation of mixed-valence U oxides (e.g. U_4O_9) formed on reduction of U(VI) by FeS.

By 1 week of sulfidation, the best fit model was 3 O backscatterers at 2.26 Å, 3 O backscatterers at 2.40 Å and 1 U backscatterer at 3.82 Å, with a notable elongation in the U-U interatomic distance, from 3.71 Å to 3.82 Å, possibly indicating a more crystalline UO_2 phase.[70] After 3 months, the best fit model contained 4 O backscatterers at 2.31 Å, 2 O backscatterers at 2.46 Å, 5 U backscatterers at 3.86 Å, and 8 distal O backscatterers at 4.42 Å. This suggests that at 3 months the U is still present as a complex mixture of nanocrystalline UO_2, mixed valence U oxide and/or U-goethite. Specifically, nanocrystalline UO_2 contains a U(IV) coordinated by 8 O ions at 2.37 Å, which is an approximate mid-point between the fitted O backscatterers at 2.31 Å and 2.46 Å. In addition, the 5 U backscatterers (3.86 Å) and 8 distal O backscatterers (4.42 Å) correlate well with nanocrystalline UO_2 (12 U at 3.87 Å, 24 O at 4.53 Å),[62] which supports the progressive U(IV) formation observed in both L_{III}-edge XANES and M_{IV}-edge HERFD-XANES. By 6 months, the best fit EXAFS model shows a marked increase in the crystallinity of the UO_2, with 5 O backscatterers at 2.32 Å, 2 O backscatterers at 2.48 Å, 8 U backscatterers at 3.86 Å, and 14 distal O backscatterers at 4.44 Å. Therefore, overall, U is partitioned to the solid phase during sulfidation and is mainly retained as nanocrystalline UO_2, with a minor amount of mixed valence U oxide and/or U-goethite.

Table 2. Details of the EXAFS fits for 1 day, 1 week, 3 months and 6 months U(VI)-goethite sulfidation samples (full details in SI, Table S2).

1 day			**1 week**			**3 months**			**6 months**		
Path	R (Å)	CN	Path	R (Å)	CN	Path	R (Å)	CN	Path	R (Å)	CN
O_1	2.24(2)	3	O_1	2.26(2)	3	O_1	2.31(1)	4	O_1	2.32(1)	5
O_2	2.38(2)	3	O_2	2.40(2)	3	O_2	2.46(2)	2	O_2	2.48(2)	2
Fe_1	3.29(3)	0.5	U_1	3.82(3)	1	U_1	3.86(1)	5	U_1	3.86(1)	8
Fe_2	3.47(4)	0.5				O_3	4.42(2)	8	O_3	4.44(1)	14
U_1	3.71(3)	1									

Reoxidation experiment. Given fluctuating redox conditions in the environment, to better understand the long-term fate of U-incorporated iron (oxyhydr)oxide phases, a controlled reoxidation experiment was performed (pH 7, 5% DO). A chemostat system was utilised to maintain the pH (*via* acid/base additions) and dissolved oxygen content (*via* air/N_2 flow), and to monitor the redox potential.

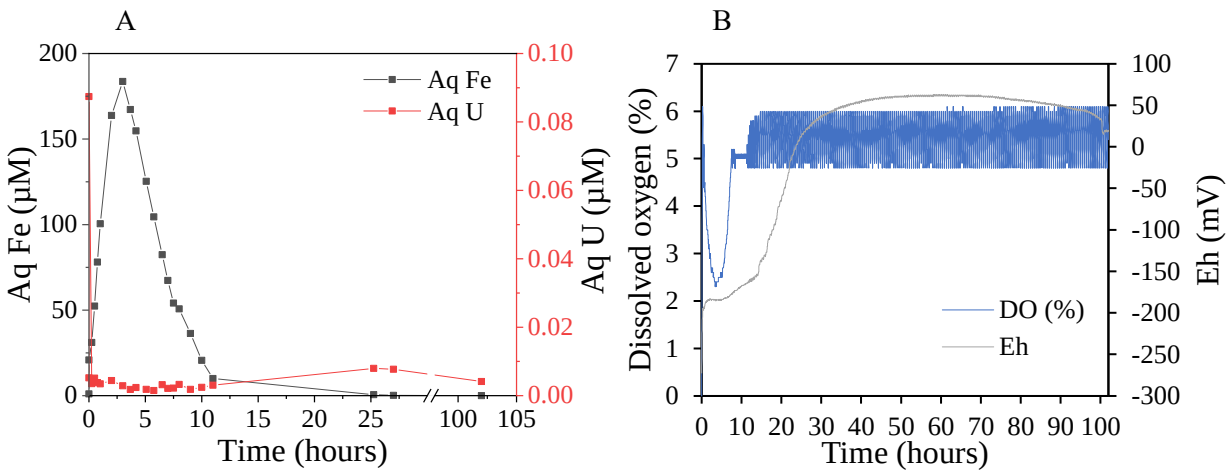

Figure 4. Solution data for the controlled reoxidation experiment. (A) Measured aqueous species; (B) redox data.

Firstly, despite a constant flow of air, DO levels initially decreased over the first 5 hours to a minimum of 2.5%, followed by a gradual increase up to the set-point of 5% DO (7.5 hours; Figure 4B). During this time, the redox potential (Eh) remained relatively low, rising only 10 mV between 1 and 7.5 hours (-187 mV to -177 mV; Figure 4B). Between 7.5 hours and 11.5 hours, minimal air and/or nitrogen was needed to maintain a DO level of 5% (Figure S5-6), with only a gradual increase of 14 mV over the 4 hours (-163 mV, 11.5 hours). However, Eh then rapidly increased, with an Eh of +2.7 mV by 24 hours. Moreover, from 11.5 hours onwards, a repeated intermittent flow of nitrogen was needed to maintain a 5% DO level, with minimal laboratory air (Figure S6).

After 4 days of oxygen ingress (at 5% DO), XRD revealed that a mixture of lepidocrocite (γ-FeOOH) and goethite (α-FeOOH) had formed in the system (Figure S14). This was confirmed by TEM images, which showed clusters of goethite rods and lepidocrocite laths (100-200 nm, Figure S12-13).[35] Therefore, the observed geochemical behaviour was likely due to the redox buffering effect of FeS, which has been shown to oxidise by the following equation:[50]

$$FeS(s) + \frac{3}{4}O_2 + \frac{1}{2}H_2O \rightarrow \frac{1}{8}S_8^0(s) + FeOOH(s)$$

In a system of synthetic nanocrystalline FeS mixed with uraninite, FeS was shown to preferentially oxidise before U(IV)O_2, thereby 'buffering' U(IV)O_2 reoxidation.[50] In the current study, the oxidation of FeS was indicated by the release of aqueous Fe, which reached a maximum concentration of 184 µM after 3 hours (Figure 4A). This was followed by a steady decrease in aqueous Fe to a minimum of 10 µM at 11 hours, likely due to the oxidation of released Fe(II), and subsequent formation of iron (oxyhydr)oxide phases (FeOOH). Therefore, the DO behaviour over the first 11 hours was likely controlled by the kinetics of FeS oxidation, which consequently buffered any rapid increase in the redox potential of the system. Furthermore, on introduction of air to the system, although there was an immediate release of 0.09 µM aqueous U (2% U), from 15 minutes onwards there was no aqueous U above the detection limit (Figure 4A). This initial U release suggests that despite the reported oxygen scavenging behaviour of synthetic nanocrystalline FeS, there may be simultaneous oxidation of the U(IV)O_2 and amorphous FeS in this system. Released U(VI) will have then immediately adsorbed and/or incorporated onto the newly formed iron (oxyhydr)oxide (FeOOH) phase.[21,71]

To assess the association of U with the iron (oxyhydr)oxide species (e.g. adsorbed or incorporated), surface bound U is often removed using techniques such as a bicarbonate extraction[17] or a sequential acid extraction.[9,15,21] Here, following 4 days of reoxidation, 65% U was found to be bicarbonate-extractable, consistent with 62% for a 0.1 M HCl extraction (Figure S15). Therefore, approximately 35% U appears to be resistant to bicarbonate or acid leaching, and is potentially incorporated within an iron (oxyhydr)oxide (i.e. goethite or lepidocrocite), with 65% U likely adsorbed to the surface.

To further probe the speciation of the U-associated iron (oxyhydr)oxide species, U L_{III}-edge XANES were collected at selected timepoints (Figure S18). The collected spectra reveal a small but progressive increase in the edge position over the first 11 hours of reaction, indicating partial U oxidation. By 4 days, there was a significant increase in the edge position, typical of a U(VI) species. This suggests that a modest fraction of U (up to ~35 % from the bicarbonate and acid leaching) may have undergone reoxidation with FeS over the first 11 hours of reaction, with subsequent incorporation into the growing iron (oxyhydr)oxide phase. The majority of U reoxidation then occurred on depletion of FeS, to form U(VI)-adsorbed iron (oxyhydr)oxides as the predominant species. In addition, XANES were collected on a sample after acid extraction of surface bound (i.e. adsorbed) U; the edge position of the U L_{III}-edge XANES decreased in energy suggesting a more reduced U species was present in the acid leached sample, where adsorbed U(VI) had been removed (Figure S18). This suggests that although the adsorbed fraction (65% U) consists of a U(VI) species, the incorporated fraction (35% U) may contain a U(V) component. Interestingly, during the sulfidation of U(VI)-incorporated goethite, there was evidence for U(V)-incorporated goethite formation (Figure 2). As a U(V)-goethite species would likely be resistant to reoxidation,[11,20] the presence of U(V)-incorporated goethite after reoxidation further supports the hypothesis that U(V)-goethite formed during U(VI)-goethite sulfidation.

The U behaviour and speciation during reoxidation was further explored using U L_{III}-edge EXAFS. Firstly, EXAFS best fits for 3-5 hours and 7.5-11 hours are very similar, with 2 O backscatterers at 2.19-2.21 Å, 4 O backscatterers at 2.37 Å and 3 U backscatterers at 3.82-3.85 Å (Table S3, SI). Therefore, although there is a slight increase in the energy of the edge position, which indicates U oxidation (Figure S18), there was still significant UO_2, and possibly mixed valence U oxides (e.g. U_4O_9), retained after 11 hours of reoxidation. By 4 days of oxygen

exposure, the EXAFS fit contains 2 O at 1.81 Å, 2 O at 2.29 Å, 2 O at 2.44 Å and 0.5 Fe at 3.44 Å, confirming that U(VI) was predominantly in a uranyl coordination. Therefore, the dominant U speciation was likely an adsorbed uranyl goethite/lepidocrocite phase, which is consistent with the chemical extraction results. Interestingly, under environmental conditions lepidocrocite is considered meta-stable, and transforms into more thermodynamically stable iron (oxyhydr)oxides, such as goethite, with time.[35] Moreover, the reaction of U(VI)-adsorbed goethite with Fe(II) has been shown to result in partial incorporation of U(V) into goethite.[16] Therefore, in the long-term, an adsorbed uranyl goethite/lepidocrocite species, as formed in this study, may transform into a U(VI)/(V)-incorporated iron (oxyhydr)oxide phase under redox cycling conditions in the sub-surface.

Environmental Implications.

Using a combination of XAS and geochemical analysis, the behaviour and speciation of U during the sulfidation, and subsequent reoxidation, of U(VI)-incorporated goethite has been explored. Initially, remobilization of a transient aqueous U species was observed, with EXAFS analysis indicating the formation of a U(VI)-persulfide species which was partially adsorbed to the solid phase at 4 hours. However, in the long term U was largely retained in the solid phase as nano-crystalline $U(IV)O_{2-x}$. Interestingly, TEM images indicated that residual U-incorporated goethite was also retained after several months. During controlled reoxidation, mackinawite then transformed to a mixed goethite/lepidocrocite phase, which contained adsorbed U(VI) (65%) and U(V/VI)-incorporated (35%) iron (oxyhydr)oxide species. These results therefore provide further support to the long-term solid phase association of U with iron (oxyhydr)oxides in both GDF and contaminated land scenarios. Although reaction with aqueous sulfide may initially release a fraction of aqueous U (e.g. 2.5%), the aqueous U species is short-lived and rapidly reduced to solid

phase UO_{2-x}. In addition, despite excess aqueous sulfide, a fraction of U(V/VI)-incorporated goethite was resistant to reductive dissolution, and partial reincorporation of U with goethite/lepidocrocite then occurred during reoxidation. Consequently, U-incorporated goethite may persist long-term under environmental conditions, including the onset of sulfate reducing conditions and the ingress of oxygen in the subsurface.

ASSOCIATED CONTENT

Supporting Information. Additional information on the geochemical analyses, M_{IV}-edge HERFD-XANES and U L_{III}-edge XAS data.

AUTHOR INFORMATION

Corresponding Author

*E-mail: sam.shaw@manchester.ac.uk

Present Addresses

†Department of Materials Science and Engineering, University of Sheffield, S1 3JD.

ORCID

Olwen Stagg: 0000-0002-3365-4110

Katherine Morris: 0000-0002-0716-7589

Luke T. Townsend: 0000-0002-7991-9444

Samuel Shaw: 0000-0002-6353-5454

Author Contributions

The manuscript was written through contributions of all authors. All authors have given approval to the final version of the manuscript.

Funding Sources

EPSRC and National Nuclear Laboratory co-funded the PhD studentship to O.S. *via* the Next Generation Nuclear CDT (EP/L0/5390/1).

Notes

The authors declare no competing financial interest.

ACKNOWLEDGMENT

Diamond Light Source provided beamtime awards (SP21441-9, SP21441-11, SP24074-7, SP24074-8, SP24074-9), and we thank Fred Mosselmanns, Shusaku Hayama, Giannantonio Cibin and Diego Gianolio for their beamline assistance. We also acknowledge access to the EPSRC NNUF RADER Facility (EP/T011300/1), ESRF beamtime, and the Leeds Electron Microscopy and Spectroscopy Centre (LEMAS) for analyses performed in this work. We thank Christopher Foster and Zabeada Aslam for assistance with data acquisition.

REFERENCES

(1) Ma, B.; Charlet, L.; Fernandez-Martinez, A.; Kang, M.; Madé, B. A Review of the Retention Mechanisms of Redox-Sensitive Radionuclides in Multi-Barrier Systems. *Appl. Geochemistry* **2019**, *100*, 414–431.

(2) Townsend, L. T.; Morris, K.; Lloyd, J. R. Microbial Transformations of Radionuclides in Geodisposal Systems. In *The Microbiology of Nuclear Waste Disposal*; Elsevier, 2021; pp

245–265.

(3) Dwivedi, D.; Steefel, C. I.; Arora, B.; Banfield, J.; Bargar, J.; Boyanov, M. I.; Brooks, S. C.; Chen, X.; Hubbard, S. S.; Kaplan, D.; Kemner, K. M.; Nico, P. S.; O'Loughlin, E. J.; Pierce, E. M.; Painter, S. L.; Scheibe, T. D.; Wainwright, H. M.; Williams, K. H.; Zavarin, M. From Legacy Contamination to Watershed Systems Science: A Review of Scientific Insights and Technologies Developed through DOE-Supported Research in Water and Energy Security. *Environ. Res. Lett.* **2022**, *17* (4), 043004.

(4) Newsome, L.; Morris, K.; Lloyd, J. R. The Biogeochemistry and Bioremediation of Uranium and Other Priority Radionuclides. *Chem. Geol.* **2014**, *363*, 164–184.

(5) Morris, K.; Law, G. T. W.; Bryan, N. D. Geodisposal of Higher Activity Wastes. In *Nuclear Power and the Environment*; Hester, R. E., Harrison, R. M., Eds.; Royal Society of Chemistry, 2011; pp 129–151.

(6) *NDA Geological Disposal - Behaviour of Radionuclides and Non-Radiological Species in Groundwater: Status Report; DSSC/456/01*; Didcot, 2016.

(7) Um, W.; Serne, R. J.; Brown, C. F.; Rod, K. A. Uranium(VI) Sorption on Iron Oxides in Hanford Site Sediment: Application of a Surface Complexation Model. *Appl. Geochemistry* **2008**, *23* (9), 2649–2657.

(8) Coutelot, F. M.; Seaman, J. C.; Baker, M. Uranium(VI) Adsorption and Surface Complexation Modeling onto Vadose Sediments from the Savannah River Site. *Environ. Earth Sci.* **2018**, *77* (4).

(9) Roberts, H. E.; Morris, K.; Law, G. T. W.; Mosselmans, J. F. W.; Bots, P.; Kvashnina, K.;

Shaw, S. Uranium(V) Incorporation Mechanisms and Stability in Fe(II)/Fe(III) (Oxyhydr)Oxides. *Environ. Sci. Technol. Lett.* **2017**, *4* (10), 421–426.

(10) Duff, M. C.; Coughlin, J. U.; Hunter, D. B. Uranium Co-Precipitation with Iron Oxide Minerals. *Geochim. Cosmochim. Acta* **2002**, *66* (20), 3533–3547.

(11) Stewart, B. D.; Nico, P. S.; Fendorf, S. Stability of Uranium Incorporated into Fe (Hydr)Oxides under Fluctuating Redox Conditions. *Environ. Sci. Technol.* **2009**, *43* (13), 4922–4927.

(12) Nico, P. S.; Stewart, B. D.; Fendorf, S. Incorporation of Oxidized Uranium into Fe (Hydr)Oxides during Fe(II) Catalyzed Remineralization. *Environ. Sci. Technol.* **2009**, *43* (19), 7391–7396.

(13) Boland, D. D.; Collins, R. N.; Payne, T. E.; Waite, T. D. Effect of Amorphous Fe(III) Oxide Transformation on the Fe(II)-Mediated Reduction of U(VI). *Environ. Sci. Technol.* **2011**, *45* (4), 1327–1333.

(14) Marshall, T. A.; Morris, K.; Law, G. T. W.; W. Mosselmans, J. F.; Bots, P.; Roberts, H.; Shaw, S. Uranium Fate during Crystallization of Magnetite from Ferrihydrite in Conditions Relevant to the Disposal of Radioactive Waste. *Mineral. Mag.* **2015**, *79* (6), 1265–1274.

(15) Doornbusch, B.; Bunney, K.; Gan, B. K.; Jones, F.; Gräfe, M. Iron Oxide Formation from $FeCl_2$ Solutions in the Presence of Uranyl (UO_2^{2+}) Cations and Carbonate Rich Media. *Geochim. Cosmochim. Acta* **2015**, *158*, 22–47.

(16) Boland, D. D.; Collins, R. N.; Glover, C. J.; Payne, T. E.; Waite, T. D. Reduction of U(VI)

by Fe(II) during the Fe(II)-Accelerated Transformation of Ferrihydrite. *Environ. Sci. Technol.* **2014**, *48* (16), 9086–9093.

(17) Massey, M. S.; Lezama-Pacheco, J. S.; Jones, M. E.; Ilton, E. S.; Cerrato, J. M.; Bargar, J. R.; Fendorf, S. Competing Retention Pathways of Uranium upon Reaction with Fe(II). *Geochim. Cosmochim. Acta* **2014**, *142*, 166–185.

(18) Marshall, T. A.; Morris, K.; Law, G. T. W.; Livens, F. R.; Mosselmans, J. F. W.; Bots, P.; Shaw, S. Incorporation of Uranium into Hematite during Crystallization from Ferrihydrite. *Environ. Sci. Technol.* **2014**, *48* (7), 3724–3731.

(19) Ilton, E. S.; Pacheco, J. S. L.; Bargar, J. R.; Shi, Z.; Liu, J.; Kovarik, L.; Engelhard, M. H.; Felmy, A. R. Reduction of U(VI) Incorporated in the Structure of Hematite. *Environ. Sci. Technol.* **2012**, *46* (17), 9428–9436.

(20) Pidchenko, I.; Kvashnina, K. O.; Yokosawa, T.; Finck, N.; Bahl, S.; Schild, D.; Polly, R.; Bohnert, E.; Rossberg, A.; Göttlicher, J.; Dardenne, K.; Rothe, J.; Schäfer, T.; Geckeis, H.; Vitova, T. Uranium Redox Transformations after U(VI) Coprecipitation with Magnetite Nanoparticles. *Environ. Sci. Technol.* **2017**, *51* (4), 2217–2225.

(21) Stagg, O.; Morris, K.; Lam, A.; Navrotsky, A.; Velázquez, J. M.; Schacherl, B.; Vitova, T.; Rothe, J.; Galanzew, J.; Neumann, A.; Lythgoe, P.; Abrahamsen-Mills, L.; Shaw, S.; Jesús, J.; Velázquez, M.; Schacherl, B.; Vitova, T.; Rothe, J.; Galanzew, J.; Neumann, A.; Lythgoe, P.; Abrahamsen-Mills, L.; Shaw, S. Fe(II) Induced Reduction of Incorporated U(VI) to U(V) in Goethite. *Environ. Sci. Technol.* **2021**, *55* (24), 16445–16454.

(22) Massey, M. S.; Lezama-Pacheco, J. S.; Michel, F. M.; Fendorf, S. Uranium Incorporation

into Aluminum-Substituted Ferrihydrite during Iron(II)-Induced Transformation. *Environ. Sci. Process. Impacts* **2014**, *16* (9), 2137–2144.

(23) Lam, A.; Hyler, F.; Stagg, O.; Morris, K.; Shaw, S.; Velázquez, J. M.; Navrotsky, A. Synthesis and Thermodynamics of Uranium-Incorporated α-Fe2O3 Nanoparticles. *J. Nucl. Mater.* **2021**, *556*, 153172.

(24) Anderson, R. T.; Vrionis, H. A.; Ortiz-Bernad, I.; Resch, C. T.; Long, P. E.; Dayvault, R.; Karp, K.; Marutzky, S.; Metzler, D. R.; Peacock, A.; White, D. C.; Lowe, M.; Lovley, D. R. Stimulating the In Situ Activity of Geobacter Species to Remove Uranium from the Groundwater of a Uranium-Contaminated Aquifer. *Appl. Environ. Microbiol.* **2003**, *69* (10), 5884–5891.

(25) Poulton, S. W.; Krom, M. D.; Raiswell, R. A Revised Scheme for the Reactivity of Iron (Oxyhydr)Oxide Minerals towards Dissolved Sulfide. *Geochim. Cosmochim. Acta* **2004**, *68* (18), 3703–3715.

(26) Zhang, S.; Peiffer, S.; Liao, X.; Yang, Z.; Ma, X.; He, D. Sulfidation of Ferric (Hydr)Oxides and Its Implication on Contaminants Transformation: A Review. *Sci. Total Environ.* **2022**, *816*, 151574.

(27) Williamson, A. J.; Morris, K.; Law, G. T. W.; Rizoulis, A.; Charnock, J. M.; Lloyd, J. R. Microbial Reduction of U(VI) under Alkaline Conditions: Implications for Radioactive Waste Geodisposal. *Environ. Sci. Technol.* **2014**, *48* (22), 13549–13556.

(28) Masters-Waage, N. K.; Morris, K.; Lloyd, J. R.; Shaw, S.; Mosselmans, J. F. W.; Boothman, C.; Bots, P.; Rizoulis, A.; Livens, F. R.; Law, G. T. W. Impacts of Repeated

Redox Cycling on Technetium Mobility in the Environment. *Environ. Sci. Technol.* **2017**, *51* (24), 14301–14310.

(29) Cumberland, S. A.; Douglas, G.; Grice, K.; Moreau, J. W. Uranium Mobility in Organic Matter-Rich Sediments: A Review of Geological and Geochemical Processes. *Earth-Science Rev.* **2016**, *159*, 160–185.

(30) Ekstrom, A. Kinetics and Mechanism of the Disproportionation of Uranium(V). *Inorg. Chem.* **1974**, *13* (9), 2237–2241.

(31) Collins, R. N.; Rosso, K. M. Mechanisms and Rates of U(VI) Reduction by Fe(II) in Homogeneous Aqueous Solution and the Role of U(V) Disproportionation. *J. Phys. Chem. A* **2017**, *121* (35), 6603–6613.

(32) Vettese, G. F.; Morris, K.; Natrajan, L. S.; Shaw, S.; Vitova, T.; Galanzew, J.; Jones, D. L.; Lloyd, J. R. Multiple Lines of Evidence Identify U(V) as a Key Intermediate during U(VI) Reduction by Shewanella Oneidensis MR1. *Environ. Sci. Technol.* **2020**, *54* (4), 2268–2276.

(33) McBriarty, M. E.; Kerisit, S.; Bylaska, E. J.; Shaw, S.; Morris, K.; Ilton, E. S. Iron Vacancies Accommodate Uranyl Incorporation into Hematite. *Environ. Sci. Technol.* **2018**, *52* (11), 6282–6290.

(34) France Lagroix, S. K. B. and M. J. J. Geological Occurrences and Relevance of Iron Oxides. In *Iron Oxides: From Nature to Applications*; Damien Faivre, Ed.; Wiley-VCH, 2016; pp 9–23.

(35) Guo, H.; Barnard, A. S. Naturally Occurring Iron Oxide Nanoparticles: Morphology,

Surface Chemistry and Environmental Stability. *J. Mater. Chem. A* **2013**, *1*, 27–42.

(36) Wan, J.; Tokunaga, T. K.; Brodie, E.; Wang, Z.; Zheng, Z.; Herman, D.; Hazen, T. C.; Firestone, M. K.; Sutton, S. R. Reoxidation of Bioreduced Uranium under Reducing Conditions. *Environ. Sci. Technol.* **2005**, *39* (16), 6162–6169.

(37) Hee, S. M.; Komlos, J.; Jaffé, P. R. Uranium Reoxidation in Previously Bioreduced Sediment by Dissolved Oxygen and Nitrate. *Environ. Sci. Technol.* **2007**, *41* (13), 4587–4592.

(38) Wu, W. M.; Carley, J.; Luo, J.; Ginder-Vogel, M. A.; Cardenas, E.; Leigh, M. B.; Hwang, C.; Kelly, S. D.; Ruan, C.; Wu, L.; Van Nostrand, J.; Gentry, T.; Lowe, K.; Mehlhorn, T.; Carroll, S.; Luo, W.; Fields, M. W.; Gu, B.; Watson, D.; Kemner, K. M.; Marsh, T.; Tiedje, J.; Zhou, J.; Fendorf, S.; Kitanidis, P. K.; Jardine, P. M.; Criddle, C. S. In Situ Bioreduction of Uranium (VI) to Submicromolar Levels and Reoxidation by Dissolved Oxygen. *Environ. Sci. Technol.* **2007**, *41* (16), 5716–5723.

(39) Canfield, D. E. Reactive Iron in Marine Sediments. *Geochim. Cosmochim. Acta* **1989**, *53*, 619–632.

(40) West, J. M.; McKinley, I. G.; Stroes-Gascoyne, S. Microbial Effects on Waste Repository Materials. In *Interactions of Microorganisms with Radionuclides*; Keith-Roach, M. J., Livens, F. R., Eds.; Elsevier, 2002; Vol. 2, pp 255–277.

(41) Kumar, N.; Pacheco, J. L.; Noël, V.; Dublet, G.; Brown, G. E. Sulfidation Mechanisms of Fe(III)-(Oxyhydr)Oxide Nanoparticles: A Spectroscopic Study. *Environ. Sci. Nano* **2018**, *5* (4), 1012–1026.

(42) Moyes, L. N.; Parkman, R. H.; Charnock, J. M.; Vaughan, D. J.; Livens, F. R.; Hughes, C. R.; Braithwaite, A.; N. Moyes, L.; H. Parkman, R.; M. Charnock, J.; J. Vaughan, D.; R. Livens, F.; R. Hughes, C.; Braithwaite, A. Uranium Uptake from Aqueous Solution by Interaction with Goethite, Lepidocrocite, Muscovite, and Mackinawite: An X-Ray Absorption Spectroscopy Study. *Environ. Sci. Technol.* **2000**, *34* (6), 1062–1068.

(43) Townsend, L. T.; Smith, K. F.; Winstanley, E. H.; Morris, K.; Stagg, O.; Mosselmans, J. F. W.; Livens, F. R.; Abrahamsen-Mills, L.; Blackham, R.; Shaw, S. Neptunium and Uranium Interactions with Environmentally and Industrially Relevant Iron Minerals. *Minerals* **2022**, *12* (2), 165.

(44) Gallegos, T. J.; Fuller, C. C.; Webb, S. M.; Betterton, W. Uranium(VI) Interactions with Mackinawite in the Presence and Absence of Bicarbonate and Oxygen. *Environ. Sci. Technol.* **2013**, *47* (13), 7357–7364.

(45) Livens, F. R.; Jones, M. J.; Hynes, A. J.; Charnock, J. M.; Mosselmans, J. F. W.; Hennig, C.; Steele, H.; Collison, D.; Vaughan, D. J.; Pattrick, R. A. D.; Reed, W. A.; Moyes, L. N. X-Ray Absorption Spectroscopy Studies of Reactions of Technetium, Uranium and Neptunium with Mackinawite. In *Journal of Environmental Radioactivity*; Elsevier, 2004; Vol. 74, pp 211–219.

(46) Townsend, L. T.; Morris, K.; Harrison, R.; Schacherl, B.; Vitova, T.; Kovarik, L.; Pearce, C. I.; Mosselmans, J. F. W.; Shaw, S. Sulfidation of Magnetite with Incorporated Uranium. *Chemosphere* **2021**, *276*, 130117.

(47) Alexandratos, V. G.; Behrends, T.; Van Cappellen, P. Fate of Adsorbed U(VI) during Sulfidization of Lepidocrocite and Hematite. *Environ. Sci. Technol.* **2017**, *51* (4), 2140–

2150.

(48) Alexandratos, V. G.; Behrends, T.; Van Cappellen, P. Sulfidization of Lepidocrocite and Its Effect on Uranium Phase Distribution and Reduction. *Geochim. Cosmochim. Acta* **2014**, *142*, 570–586.

(49) Townsend, L. T.; Shaw, S.; Ofili, N. E. R.; Kaltsoyannis, N.; Walton, A. S.; Frederick, J.; Mosselmans, W.; Neill, T. S.; Lloyd, J. R.; Heath, S.; Hibberd, R.; Morris, K. Formation of a U(VI)−Persulfide Complex during Environmentally Relevant Sulfidation of Iron (Oxyhydr)Oxides. *Environ. Sci. Technol.* **2020**, *54* (1), 129–136.

(50) Bi, Y.; Hyun, S. P.; Kukkadapu, R.; Hayes, K. F. Oxidative Dissolution of UO2 in a Simulated Groundwater Containing Synthetic Nanocrystalline Mackinawite. *Geochim. Cosmochim. Acta* **2013**, *102*, 175–190.

(51) Sherman, D. M.; Peacock, C. L.; Hubbard, C. G. Surface Complexation of U(VI) on Goethite (α-FeOOH). *Geochim. Cosmochim. Acta* **2008**, *72* (2), 298–310.

(52) Guo, Z.; Li, Y.; Wu, W. Sorption of U(VI) on Goethite: Effects of PH, Ionic Strength, Phosphate, Carbonate and Fulvic Acid. *Appl. Radiat. Isot.* **2009**, *67* (6), 996–1000.

(53) Fonselius, S.; Dyrssen, D.; Yhlen, B. Determination of Hydrogen Sulphide. In *Methods of Seawater Analysis*; Wiley-VCH Verlag GmbH, 1999; pp 91–100.

(54) Ravel, B.; Newville, M. ATHENA, ARTEMIS, HEPHAESTUS: Data Analysis for X-Ray Absorption Spectroscopy Using IFEFFIT. *J. Synchrotron Radiat.* **2005**, *12* (4), 537–541.

(55) Scheinost, A. C.; Claussner, J.; Exner, J.; Feig, M.; Findeisen, S.; Hennig, C.; Kvashnina, K. O.; Naudet, D.; Prieur, D.; Rossberg, A.; Schmidt, M.; Qiu, C.; Colomp, P.; Cohen, C.;

Dettona, E.; Dyadkin, V.; Stumpf, T. ROBL-II at ESRF: A Synchrotron Toolbox for Actinide Research. *J. Synchrotron Radiat.* **2021**, *28*, 333–349.

(56) Kvashnina, K. O.; Scheinost, A. C.; Beamline, R. A Johann-Type X-Ray Emission Spectrometer at the Rossendorf Beamline. *J. Synchrotron Radiat.* **2016**, *23*, 836–841.

(57) Kvashnina, K. O.; Butorin, S. M.; Martin, P.; Glatzel, P. Chemical State of Complex Uranium Oxides. *Phys. Rev. Lett.* **2013**, *111* (25), 253002.

(58) Kvashnina, K. O.; Butorin, S. M. High-Energy Resolution X-Ray Spectroscopy at Actinide M4,5 and Ligand K Edges: What We Know, What We Want to Know, and What We Can Know. *Chem. Commun.* **2022**, *58* (3), 327–342.

(59) Roßberg, A.; Reich, T.; Bernhard, G. Complexation of Uranium(VI) with Protocatechuic Acid-Application of Iterative Transformation Factor Analysis to EXAFS Spectroscopy. *Anal. Bioanal. Chem.* **2003**, *376* (5), 631–638.

(60) Poulton, S. W. Sulfide Oxidation and Iron Dissolution Kinetics during the Reaction of Dissolved Sulfide with Ferrihydrite. *Chem. Geol.* **2003**, *202* (1–2), 79–94.

(61) Kaminski, M. D.; Dimitrijevic, N. M.; Mertz, C. J.; Goldberg, M. M. Colloids from the Aqueous Corrosion of Uranium Nuclear Fuel. *J. Nucl. Mater.* **2005**, *347* (1–2), 77–87.

(62) Neill, T. S.; Morris, K.; Pearce, C. I.; Sherriff, N. K.; Burke, ⊥ M Grace; Chater, P. A.; Janssen, A.; Natrajan, L.; Shaw, S. Stability, Composition, and Core−Shell Particle Structure of Uranium(IV)-Silicate Colloids. **2018**.

(63) Matamoros-Veloza, A.; Cespedes, O.; Johnson, B. R. G.; Stawski, T. M.; Terranova, U.; de Leeuw, N. H.; Benning, L. G. A Highly Reactive Precursor in the Iron Sulfide System.

Nat. Commun. **2018**, *9* (1), 1–7.

(64) Ohfuji, H.; Rickard, D. High Resolution Transmission Electron Microscopic Study of Synthetic Nanocrystalline Mackinawite. *Earth Planet. Sci. Lett.* **2006**, *241* (1–2), 227–233.

(65) Pan, Z.; Bártová, B.; LaGrange, T.; Butorin, S. M.; Hyatt, N. C.; Stennett, M. C.; Kvashnina, K. O.; Bernier-Latmani, R. Nanoscale Mechanism of UO2 Formation through Uranium Reduction by Magnetite. *Nat. Commun.* **2020**, *11* (1), 4001.

(66) Hua, B.; Deng, B. Reductive Immobilization of Uranium(VI) by Amorphous Iron Sulfide. *Environ. Sci. Technol.* **2008**, *42* (23), 8703–8708.

(67) Docrat, T. I.; Mosselmans, J. F. W.; Charnock, J. M.; Whiteley, M. W.; Collison, D.; Livens, F. R.; Jones, C.; Edmiston, M. J. X-Ray Absorption Spectroscopy of Tricarbonatodioxouranate(V), [UO2(CO3)3]5-, in Aqueous Solution. *Inorg. Chem.* **1999**, *38* (8), 1879–1882.

(68) Tewari, P. H.; McLean, A. W. Temperature Dependence of Point of Zero Charge of Alumina and Magnetite. *J. Colloid Interface Sci.* **1972**, *40* (2), 267–272.

(69) Jones, D. J.; Roziere, J.; Allen, G. C.; Tempest, P. A. The Structural Determination of Fluorite-Type Oxygen Excess Uranium Oxides Using EXAFS Spectroscopy. *J. Chem. Phys* **1986**, *84* (11), 6075–6082.

(70) Middleburgh, S. C.; Lee, W. E.; Rushton, M. J. D. Structure and Properties of Amorphous Uranium Dioxide. *Acta Mater.* **2021**, *202*, 366–375.

(71) McBriarty, M. E.; Soltis, J. A.; Kerisit, S.; Qafoku, O.; Bowden, M. E.; Bylaska, E. J.; De

Yoreo, J. J.; Ilton, E. S. Trace Uranium Partitioning in a Multiphase Nano-FeOOH System. *Environ. Sci. Technol.* **2017**, *51* (9), 4970–4977.